An Integrated Electrochromic Nanoplasmonic Optical Switch

Amit Agrawal[1,2], Ceren Susut[1], Gery Stafford[3], Ugo Bertocci[3], Ben McMorran[1], Henri Lezec[1] and A. Alec Talin[1]*

[1]Center for Nanoscale Science and Technology, National Institute of Standards and Technology, Gaithersburg, MD 20899

[2]Maryland Nanocenter, University of Maryland, College Park, MD 20742, (USA)

[3]Measurement and Materials Laboratory, National Institute of Standards and Technology Gaithersburg, MD 20899

*E-mail: atalin@nist.gov

RECEIVED DATE (to be automatically inserted after your manuscript is accepted if required according to the journal that you are submitting your paper to)

We demonstrate an electrochemically-driven optical switch based on absorption modulation of surface plasmon polaritons (SPPs) propagating in a metallic nanoslit waveguide containing electrochromic Prussian Blue (PB) nanocrystals. Optical transmission modulation of≈96 % is achieved by electrochemically switching the dye between its oxidized and reduced states using voltages below 1 V. High spatial overlap and long interaction length between the SPP and the active material is achieved by preferential growth of PB nanocrystals on the nanoslit sidewalls. In addition, the resulting orthogonalization between the directions of light propagation, and that of charge transport from the electrolyte to ultra-thin active material inside the nanoslit waveguide offers significant promise for the realization of electrochromic devices with record switching speeds.

Keywords: Plasmonics, Electrochromic, Optical Switch, Nanoslit, Electrochemical Deposition

The understanding and control of the interaction of light with matter is fundamental to science and technology. Such an understanding has led to the development of lasers and optical fibers which form the backbone of modern communication systems. In addition, significant advances in nanofabrication techniques over the last few years have made it possible to fabricate sophisticated optical devices with greater functionality at subwavelength dimensions. However, active control of light propagation at subwavelength scales still remains a challenge. During the last decade there has been tremendous interest in using optical devices based on surface plasmon polaritons (SPPs) for subwavelength control of light [1]. SPPs are collective charge oscillations coupled to an external electromagnetic field that propagate along an interface between a metal and a dielectric [2]. It is the mixed nature of SPPs and their dependence on the index of refraction of the dielectric medium facing the metal which forms the basis for their application to chemical and biological sensing, a technique broadly known as surface plasmon resonance (SPR) spectroscopy [3]. In addition, active control of SPPs has previously been demonstrated by purely mechanical means [4], electro-mechanical transduction [5] or by manipulating the dielectric refractive index either optically or electrically using liquid crystals [6-8], quantum dots [9], nonlinear optical materials [10, 11] or photochromic dyes [12]. The weak nonlinearity of the metal itself has also been utilized in planar or nanostructured geometries for ultrafast active plasmonic applications [13, 14]. However, these approaches either require large pump fluences (several mJ/cm^2) [11, 13, 14], relatively high voltages (>10 V) [6, 8, 10], multiple control wavelengths [12], or achieve only modest On/Off contrast ratios (<3:1) [7, 9].

In addition to devices exploiting propagating SPPs, there has also been strong interest in recent years in applications based on stationary charge-oscillation resonances in metallic

nanostructures known as localized surface plasmons (LSP) [15]. For example, active tuning of LSP resonances has been demonstrated in the case of Au nanoparticles imbedded in a conducting polymer matrix, by electrochemically changing the electronic state of the polymer [16]. Compared to nanoparticle-based devices sustaining stationary LSP resonances, however, metallic cavity waveguide devices sustaining propagating SPPs readily offer the advantages of both deep-subwavelength mode confinement and increased interaction length with active materials [1].

In this Letter, we demonstrate an electrochemically-driven optical switch based on absorption modulation of SPPs propagating in a metallic nanoslit waveguide containing electrochromic Prussian Blue nanocrystals. The nanocrystals are preferentially grown on the slit waveguide sidewalls using cyclic voltammetry deposition. Optical transmission modulation of≈96 % (On/Off contrast ratio ≈20:1) is achieved by electrochemically switching the dye between its Prussian Blue (PB) oxidized state and Prussian White (PW) reduced state using voltages below 1 V. Such a large transmission modulation is enabled by both the high spatial overlap and long interaction length between the SPP and the PB nanocrystals inside the nanoslit waveguide.

Experimental devices were fabricated on fused silica substrates coated with a 2 nm thick Ti adhesion layer. A nanoslit-patterned sample (Sample A) was formed by evaporation of an optically thick Au film of thickness 250 nm on one of the fused silica substrates. Rectangular slits of width 50 nm and length 5 μm were then milled through the Au film using a focused ion beam (FIB). A scanning electron microscope (SEM) image of one of the nanoslits of Sample A is shown in Fig. 1a. In addition, a semi-transparent unpatterned reference sample (Sample B) was formed by evaporating a Au film of thickness 30 nm with a 2 nm Ti adhesion layer on another fused silica substrate. Samples A and B were then used as working electrodes (‘WE’) in a spectro-electrochemical cell (Fig. 1b). An o-ring of diameter

15 mm, clamped between the substrate and the body of the cell to form a water-tight seal, defined the geometric area of the working electrode. PB deposition on Samples A and B was carried out in an electrolyte solution containing 5 mM $K_4Fe(CN)_6$ in 0.1 M $HClO_4$ using a saturated sulfate reference electrode (SSE) ('RE' in Fig. 1b), separated by a Luggin capillary, and a coiled Pt wire counter electrode ('CE' in Fig. 1b). Following deposition, electrochromic switching experiments between PB and PW states were carried out using a 0.1 M KNO_3 electrolyte. A microscope connected to a spectrometer/Si CCD camera was used to measure the optical transmission of Samples A and B under normal incidence illumination at λ_0=633 nm. In the case of Sample A the incident light was polarized with electric field orthogonal to the slit length. The optical transmission and the working electrode current were recorded simultaneously during the ferrocyanide/ferricyanide redox reaction as the potential was cycled between -0.8 V to 0.7 V (SSE).

A series of cyclic voltammograms (CVs) were performed using the semitransparent reference Sample B facing a solution of $K_4Fe(CN)_6$ in 0.1 M $HClO_4$ (Fig. 2a) while simultaneously monitoring the optical transmission (Fig. 2c). The first CV is typical of a ferricyanide/ferrocyanide redox couple. However, on the sixth cycle, a small peak emerges at ≈-0.4 V (SSE) on the cathodic sweep. After 300 cycles, additional peaks located at ≈-0.4 V (SSE) and ≈0.35 V (SSE) are clearly visible. The location of these peaks is consistent with the published redox behavior of PB (ferric ferrocyanide or $KFe_2(CN)_6$). The characteristic deep blue color of the dye in the PB state is due to charge transfer from the carbon surrounded Fe(II) to the nitrogen surrounded Fe(III) [17]. Reduction of PB is accomplished by diffusion of electrons (from Au) and K^+ ions (from solution) into the film, leading to conversion of the PB into $K_2Fe_2(CN)_6$, commonly known as Prussian White (PW) or Everitt's salt, while oxidation of PB is accomplished by out-diffusion of electrons and ions, leading to conversion of the PB into $Fe_2(CN)_6$, commonly known as Berlin green (BG) [17].

Deposition of PB by CV on Au or Pt working electrodes from a weakly acidic ferricyanide ($K_3Fe(CN)_6$) solution has previously been reported along with a general description of the deposition mechanism [18, 19]. The ferricyanide dissociates into free ferric ions according to the following reaction,

$$Fe(CN)_6^{3-} + 6H^+ \Leftrightarrow Fe^{3+} + 6HCN \uparrow , \qquad (1)$$

so that a mixture of ferric and ferricyanide is present in solution. Dissociation is strongly pH dependent which partially explains why PB deposition is favored in acidic solutions. On the first cathodic cycle, both the ferric and ferricyanide are reduced to ferrous and ferrocyanide. Ferrocyanide ion reacts with ferrous ion in the presence of K^+ to form PW on the electrode working electrode surface. PW is then converted to PB upon oxidation. The extremely low ferric ion concentration leads to a dense and crystalline layer of PB. The deposition rate can be quantified by integrating the PB/PW reduction current, assuming the following electrochemical reaction,

$$KFe^{III}Fe^{II}(CN)_6 + e^- + K^+ \Leftrightarrow K_2Fe^{II}Fe^{II}(CN)_6 \ . \qquad (2)$$

We have examined the data in Fig. 2a and 2b and have determined that on average each cycle generates about 4 x 10^{-11} mol/cm^2 of $KFeFe(CN)_6$, which corresponds to approximately 0.1 monolayers. Based on this growth rate, 200 cycles would produce a film of thickness ≈25 nm , assuming uniform deposition. Note that the CVs collected for Samples B (Fig. 2a) and A (Fig. 2b) are nearly identical, indicating that deposition of PB progressed in a similar manner for the two Au substrates.

During the anodic sweep the transmitted optical intensity measured through both semitransparent reference Samples B (Fig. 2c) and nanoslit patterned Sample A (Fig. 2d) is observed to drop from a more transmissive state below -0.4 V to a more absorbing state between 0 V to 0.2 V, consistent with switching of the dye from its PW to the PB state. We define I_{ON} and I_{OFF} as the transmitted light intensity at voltages of -0.8 V and at 0 V, which are representative of the PW and PB states, respectively, yielding a switching contrast defined as $\gamma = (I_{ON}-I_{OFF})/I_{ON}$. For both Samples A and B, γ increases as number of cycles, reaching a maximum asymptotic value of ≈30 % after 200 cycles for Sample B and ≈96 % after only 51 cycles for Sample A. In the case of Sample A, in contrast to that of sample B, optical switching between ≈-0.4 V (SSE) and ≈0.35 V (SSE), consistent with the PB redox transitions, is evident even on the first cycle (Fig. 2d) corresponding to a γ of ≈30 %. Note that the noise in the optical signal corresponds to 3 % of the intensity at one standard deviation. Normal incidence SEM images of reference Sample B after 300 cycles of deposition and nanoslit patterned Sample A after 51 cycles are shown in Fig. 2e and 2f, respectively. Sample B appears nearly completely covered with cubic crystallites ranging in width from a few to over one hundred nanometers. In the case of Sample A, PB is observed to initially deposit preferentially on the nanoslit sidewalls. Preferential deposition in the nanoslit was further confirmed by high resolution SEM imaging at 52° sample tilt (Fig. S1), as well as by scanning Auger electron spectroscopy collected following several cycles of deposition (Fig. S2). X-ray diffraction collected on both Samples A and B confirmed that the cubic nanoparticles were (100) oriented PB crystallites (see supporting info Fig. S3). We estimate that the fill fraction of PB crystallites in the nanoslits of Sample A reaches a maximum value of ≈0.25 after ≈50 deposition cycles, with further cycling leading to PB growth on the top Au surface. The observed saturation in fill fraction explains why γ does not increase with further cycling. The optical switching performance of Samples A and B is

summarized in Fig. 3, where the switching contrast γ is plotted versus the number of deposition cycles for both cases.

The high contrast ratio we report cannot be explained using a simple path length argument. To understand the origin of the large magnitude of the observed switching contrast, finite difference time domain (FDTD) simulations were used to replicate light transmission through a nanoslit containing dye nanocrystals switched between PW and PB states. Two - dimensional FDTD simulations were performed using normally-incident continuous-wave light of wavelength λ_0=633 nm polarized orthogonal to a 50 nm wide slit in a 250 nm thick Au film on glass immersed in an aqueous environment of index of refraction 1.33. Dye nanocrystals were modeled as 20 nm × 20 nm squares evenly distributed on the slit sidewalls, with a slit fill fraction of 25 %. The indices of refraction used to model PW and PB states, respectively n_{PW} = 1.371 and n_{PB} = 1.371 + i 0.186, were obtained from literature values for PB in bulk form [20]. As expected, simulations reveal that the presence of SPP modes in the slit with intensity maxima concentrated on the slit sidewalls. Simulated transmitted light intensities under PW and PB nanocrystal states, respectively I_{PW} and I_{PB}, yield a theoretical switching contrast $\gamma_{FDTD} = (I_{PW} - I_{PB}) / I_{PW}$ = 33.8%, which is significantly smaller then the measured switching contrast $\gamma \approx 96$ % shown in Fig. 3. The measured value γ could be matched in simulation by setting n_{PB} = 1.371 + i 1.5, in other words assuming an eight-fold increase in the imaginary part of the index of refraction of PB compared to published bulk data. The origin of this anomalously-high absorption coefficient for PB nanocrystals formed on Au surfaces is currently under investigation.

In summary, we demonstrate an electrochromic optical switch consisting of nanocrystals of Prussian Blue dye electrochemically deposited in a nanoslit plasmonic waveguide, and electrochemically switched between absorptive and transmissive states. High switching contrast, evidenced here by measurements at λ_0=633 nm, is enabled via strong

spatial interaction between light and active material under the respective form of SPPs propagating along the surface of the slit sidewalls and a thin layer of PB nanocrystals located on the same surface. Device switching contrast is further enhanced by the anomalously large intrinsic absorption coefficient found to characterize PB nanocrystals grown on a Au surface. As a result, the switch is able to operate efficiently under conditions of a relatively low fill fraction of active material in the slit (≈25 %), leading to large contact area with the electrolyte. The resulting orthogonalization between the directions of light propagation, parallel to the depth of the slit, and that of charge transport from the electrolyte to ultra-thin active material, largely parallel to the width of the slit, offers significant promise for the realization of electrochromic devices with record switching speeds.

References

[1] S. A. Maier, *Plasmonics: Fundamentals and Applications*, (Springer, New York, 2007) and references therein.
[2] H. Raether, *Surface Plasmons on Smooth and Rough Surfaces and on Gratings*, (Vol. 111 of Springer Tracts in Modern Physics, Springer-Verlag, Berlin, 1988).
[3] J. Homola, *Chem. Rev.* **2008**, 108, 462.
[4] F. Huang and J. J. Baumberg, *Nano Lett.* **2010**, 10, 1787.
[5] J. L. Skinner, A. A. Talin, and D. A. Horsley, *Opt. Express* **2008**, 16, 3701.
[6] T. J. Kim, T. Thio, T. W. Ebbesen, D. E. Grupp, and H. J. Lezec, *Opt. Lett.* **1999**, 24, 256.
[7] V. K. S. Hsiao, Y. B. Zheng, B. K. Juluri, T. J. Huang, *Adv. Mater.* **2008**, 20, 3528.
[8] W. Dickson, G. A. Wurtz, P. R. Evans, R. J. Pollard, A. V. Zayats, *Nano Lett.* **2008**, 8, 281.
[9] D. Pacifici, H. J. Lezec, and H. A. Atwater, *Nat. Photon.* **2007**, 1, 402.
[10] M. J. Dicken, L. A. Sweatlock, D. Pacifici, H. J. Lezec, K. Bhattacharya, and H. A. Atwater, *Nano Lett.* **2008**, 8, 4048.
[11] C. Min, P. Wang, C. Chen, Y. Deng, Y. Lu, H. Ming, T. Ning, Y. Zhou, and G. Yang, *Opt. Lett.* **2008**, 33, 869.
[12] R. A. Pala, K. T. Shimizu, N. A. Melosh, and M. L. Brongersma, *Nano Lett.* **2008**, 8, 1506.
[13] K. F. MacDonald, Z. L. Samson, M. I. Stockman, and N. I. Zheludev, *Nat. Photonics* **2009,** 3, 55.
[14] G. A. Wurtz, R. Pollard, W. Hendren, G. P. Wiederrecht, D. J. Gosztola, V. A. Podolskiy and A. V. Zayats, *Nat. Nanotechnology* **2011**, 6, 107.
[15] K. A. Willets and R. P. Van Duyne, *Annu. Rev. Phys. Chem.* **2007,** 58, 267.
[16] V. Stockhausen, P. Martin, J. Ghilane, Y. Leroux, H. Randriamahazaka, J. Grand, N. Felidj, J. C. Lacroix, *J. Amer. Chem. Soc.* **2010**, 132, 10224.
[17] K. Itaya, I. Uchida, V. D. Neff, Acc. Chem. Res. **1986**, 19, 162.
[18] R. Yang, Z. B.Qian, J. Q. Deng, *J. Electrochem. Soc.* **1998**, *145*, 2231.

[19]D. Zhang, K. Wang, D. C. Sun, X. H. Xia, H.-Y. Chen, *Chem. Mater.* **2003**, *15*, 4163.
[20] S. Cowen, J. Sambles, and A. Glidle, *Journal of Electroanalytical Chemistry* **1989**, 261, 455.

Figure Captions.

Figure 1. (a) SEM image of nanoslit fabricated in a 250 nm thick Au film on fused silica using focused ion beam (FIB) milling. (b) Schematic of the experimental setup showing the electrochemical cell integrated with the nanoplasmonic devices for transmission measurements. RE, CE and WE correspond to the reference electrode, counter electrode and working electrode respectively.

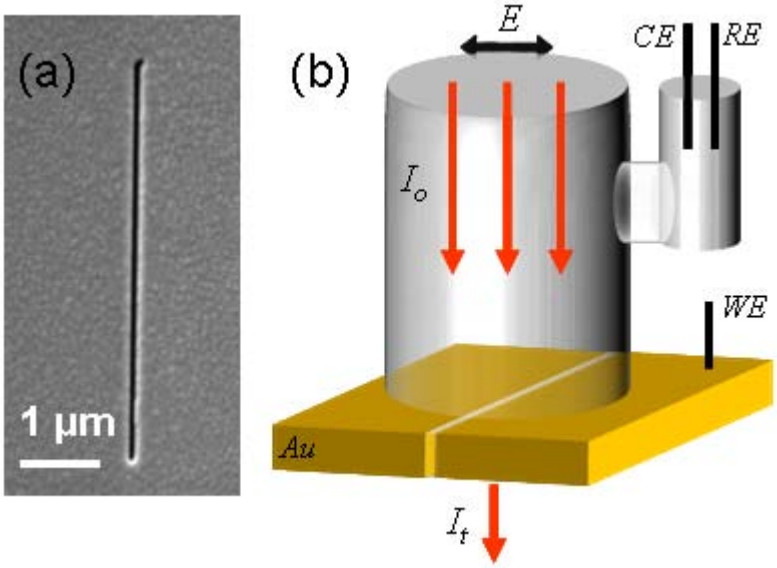

Figure 2. Series of four cyclic voltammograms in the $K_4Fe(CN)_6$ in 0.1 M $HClO_4$ solution collected with (a) 30 nm thick unpatterned reference gold electrode and (b) nanoslit patterned 250 nm gold electrode. Additional peaks at ≈-0.4 V (SSE) and ≈0.35 V (SSE) at higher number of cycles consistent with the redox behavior of PB are clearly evident. Corresponding normlized optical transmission through the (c) 30 nm thick gold electrode (Sample B) and (d) nanoslit patterned 250 nm gold electrode (Sample A). The purple arrow in (b) and (d) corresponds to the potential sweep during the anodic cycle. SEM image of the (e) 30 nm thick unpatterned gold after 300 cycles and (f) nanoslit device on 250 nm thick gold after 51 cycles. Preferential PB nanocrystal growth in the nanoslit cavity is clearly evident in (f).

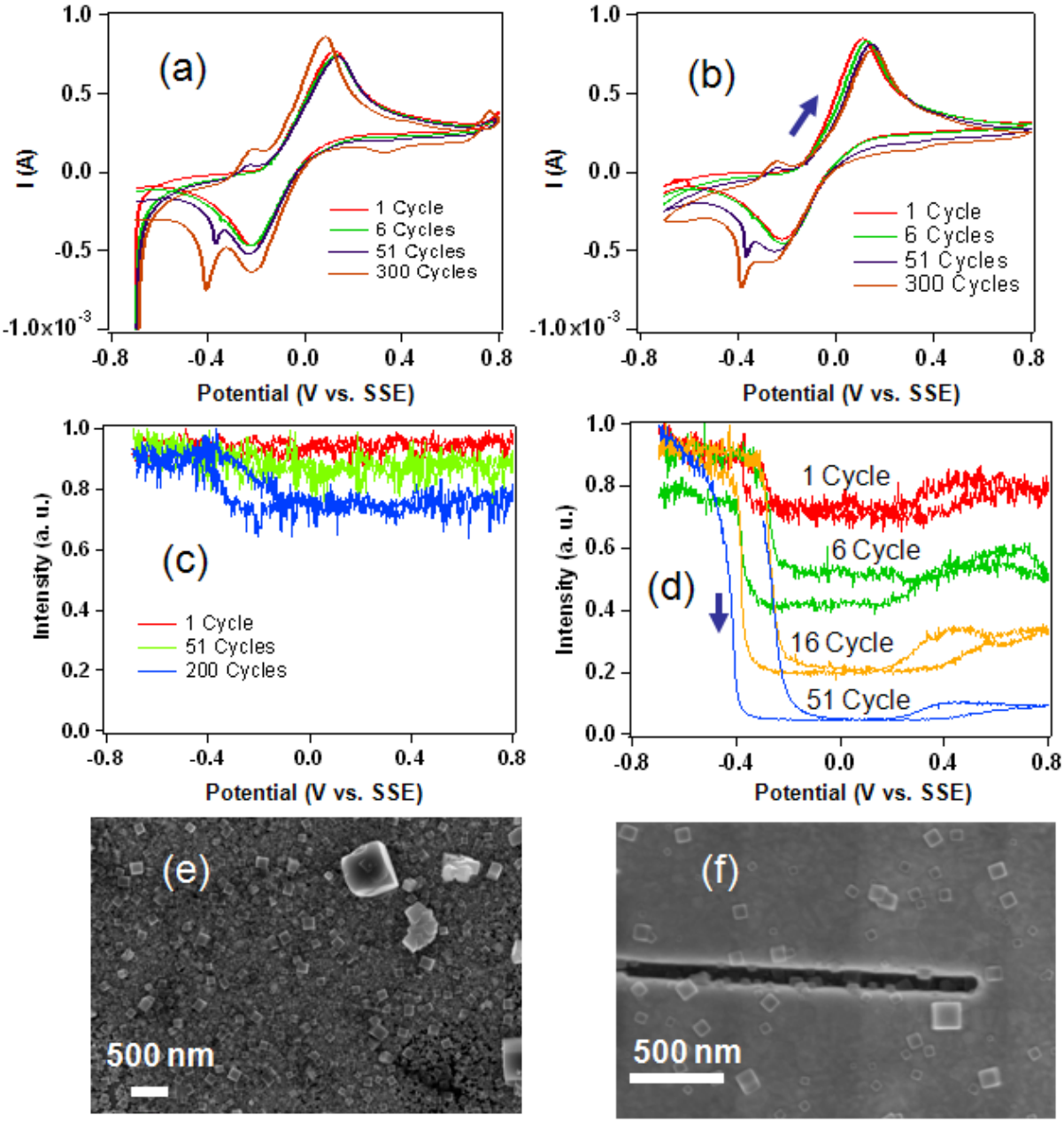

Figure 3. Switching contrast (γ) as a function of number of cycles extracted from the transmission measurements in Fig. 2. The blue and the red curve correspond to γ through the semitransparent reference Sample B and the nanoslit patterned sample A, respectively. Significantly higher switching contrast associated with the PB nanocrystal decorated nanoslit is clearly evident. The error bars represent the standard deviation of the variation in recorded intensity resulting from the detector noise (silicon CCD).

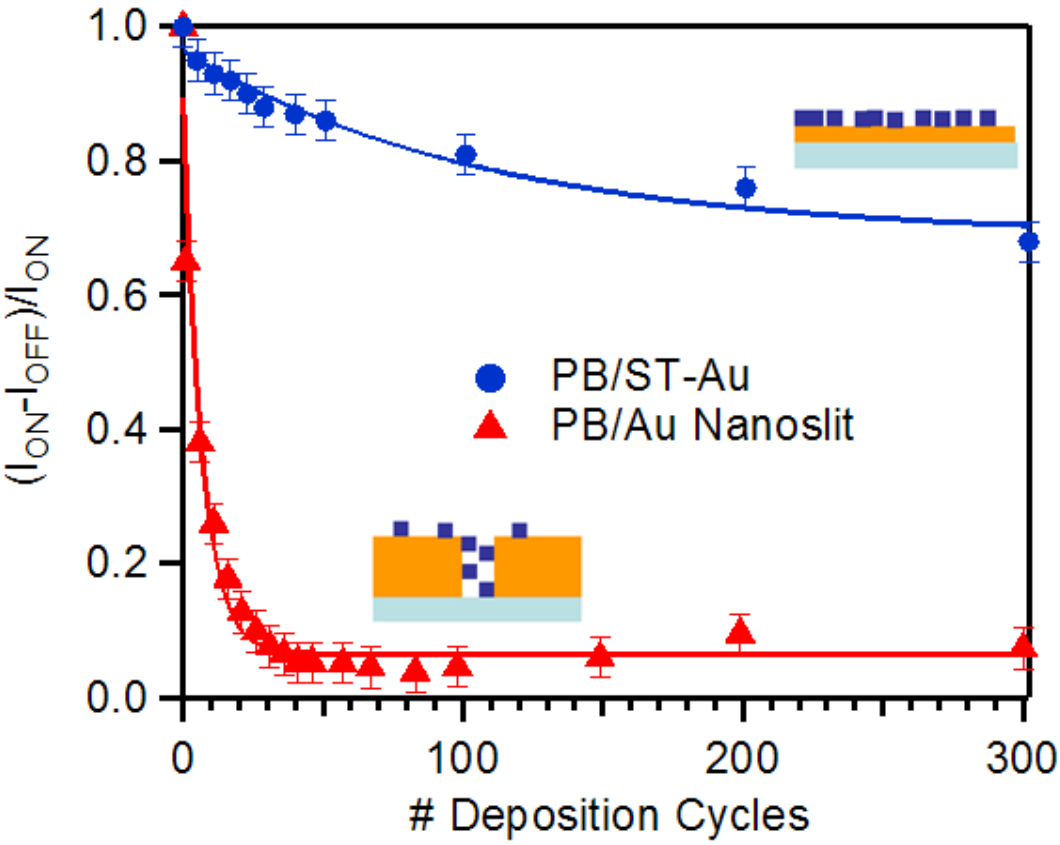

SUPPLEMENTRY INFORMATION

An Integrated Electrochromic Nanoplasmonic Optical Switch

*By Amit Agrawal, Ceren Susut, Gery Stafford, Ugo Bertocci, Ben McMorran, Henri Lezec and A. Alec Talin**

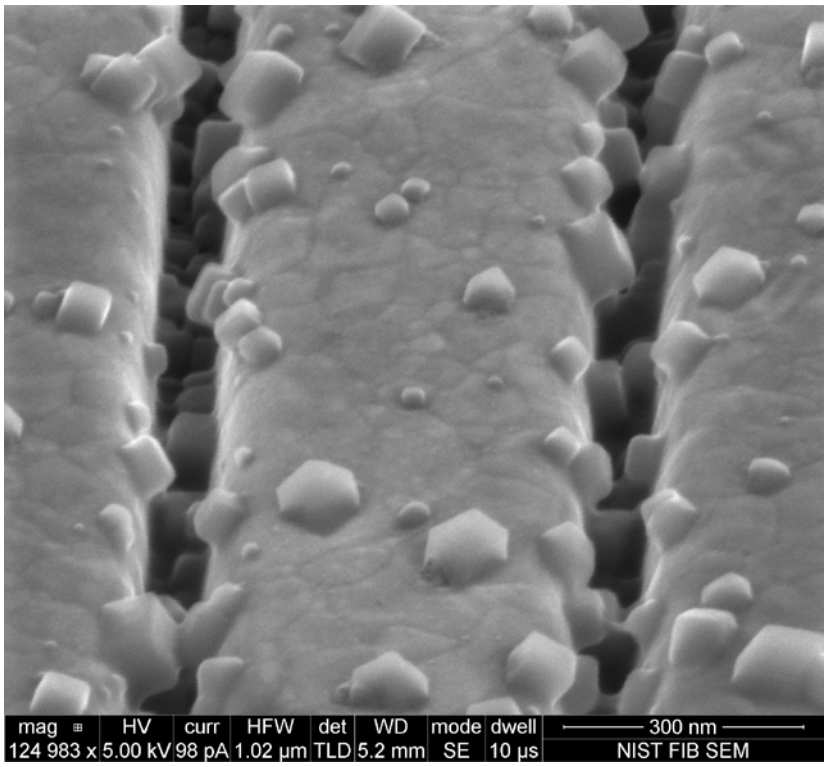

Figure S1. High resolution secondary electron microscope (SEM) image of two adjacent slits of width 50 nm milled through 250 nm thick gold after 51 cycles of PB deposition. The individual slit dimensions are identical to those used in the switching experiments. Low fill fraction (< ≃25 %) as well as preferential deposition of PB nanocrystals on the slit side walls is clearly evident.

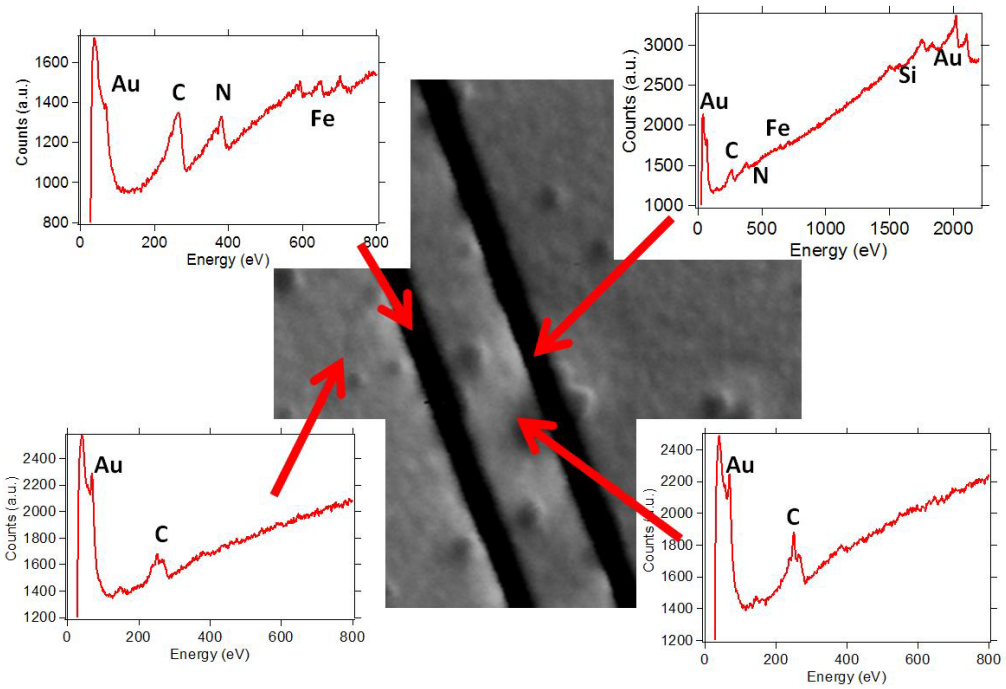

Figure S2. Auger Electron Microscope image of double slit structure milled in 250 nm thick gold film after 5 cycles of Prussian Blue (PB) deposition. Elemental maps plotted as Insets clearly demonstrate preferential deposition of PB inside the nanoslits.

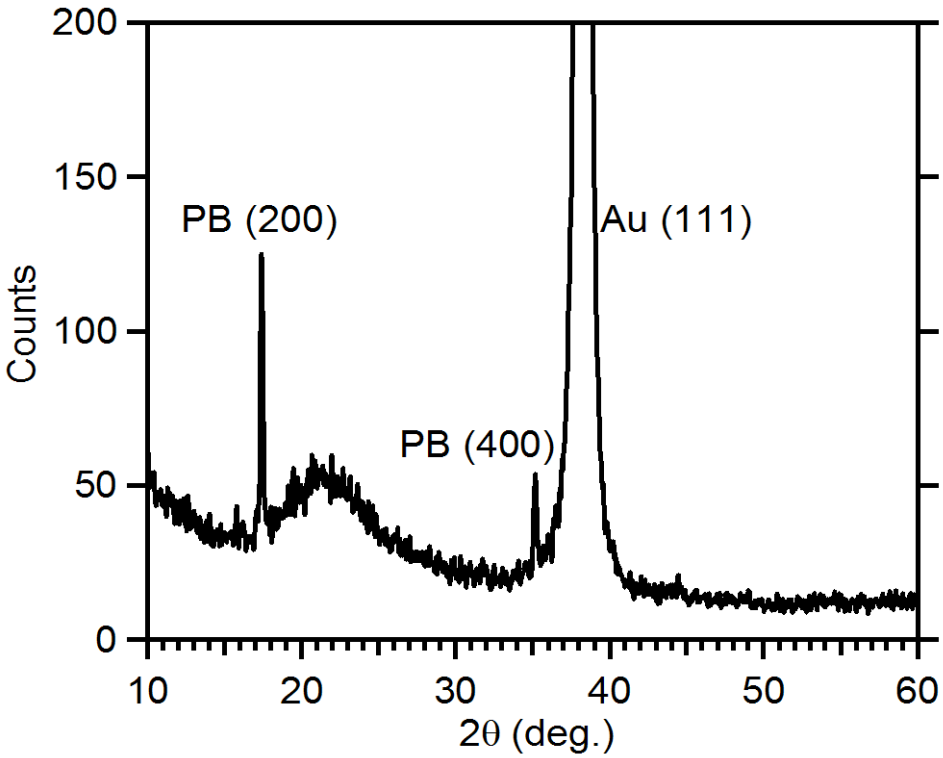

Figure S3. X-ray diffraction pattern of Prussian Blue (PB) deposited on a semitransparent reference Au substrate (Sample B) after 300 cycles collected using a powder diffractometer and Cu K-alpha x-rays (0.154 nm).